INTERNATIONAL JOURNAL OF CLIMATOLOGY
Int. J. Climatol. **34**: 3499–3514 (2014)
Published online 12 February 2014 in Wiley Online Library
(wileyonlinelibrary.com) DOI: 10.1002/joc.3923

RMetS
Royal Meteorological Society

Temporal and spatial variability of frost-free seasons in the Great Lakes region of the United States

Lejiang Yu,[a]* Shiyuan Zhong,[b] Xindi Bian,[c] Warren E. Heilman[c] and Jeffrey A. Andresen[b]

[a] *Applied Hydrometeorological Research Institute, Nanjing University of Information Science and Technology, China*
[b] *Department of Geography and Center for Global Change and Earth Observations, Michigan State University, East Lansing, MI, USA*
[c] *USDA Forest Service Northern Research Station, East Lansing, MI, USA*

ABSTRACT: The frequency and timing of frost events and the length of the growing season are critical limiting factors in many human and natural ecosystems. This study investigates the temporal and spatial variability of the date of last spring frost (LSF), the date of first fall frost (FFF), and the length of the frost-free season (FFS) in the Great Lakes region of the United States using two gridded reanalysis datasets for the period of 1980–2010. Across most of the Great Lakes region, there has been a negative trend for the LSF and a positive trend for the FFF, leading to a lengthening of FFS. The three variables vary spatially across the region and exhibit large interannual variability. Empirical orthogonal function (EOF) analyses indicate that the first mode for the three variables, which accounts for about 30% of the total variance, is in phase across most of the Great Lakes region and that it appears to be related to Pacific North American (PNA) pattern in the case of LSF and to Pacific Decadal Oscillation (PDO) in the case of FFF and FFS. The main reason for these connections is that the 200-hPa geopotential height anomaly over North America induced by a Rossby wave train influences the strength of the trough over North America, which in turn affects surface temperatures over the Great Lakes region. The second mode, explaining about 10% of the total variance, mainly shows the out-of-phase variability between the Great Lakes and the surrounding land and it appears to be related to the circumglobal teleconnection (CGT) in the case of LSF and again to PDO in the case of FFF and FFS.

KEY WORDS frost dates; frost-free season; the Great Lakes region; Pacific Decadal Oscillation

Received 30 May 2013; Revised 11 December 2013; Accepted 19 December 2013

1. Introduction

The frost-free season (FFS) is defined as the period between the last spring freeze and the first fall freeze. The longer the FFS is, the longer the growing season will be. The length of the FFS influences strongly not only the growth of plants and seasonal activities of animals, but also the hydrological cycle and human activities (Zhou *et al.*, 2001; Cotton, 2003; Groisman *et al.*, 2004; Nicholls, 2005).

Previous researchers have investigated changes in the number of frost-free days in United States over different time periods. Cooter and LeDuc (1995) documented a significant increasing trend in the length of the FFS in the northeastern United States for the period 1961–1990 and indicated that the trend may be related to changes in the amount of sunshine and cloud cover. DeGaetano (1996) found a decreasing trend in days with minimum temperature of less than or equal to −15.0 °C in the northeastern Unite States over the period of 1959–1993. Schwartz and Reiter (2000) detected a 5–6 day move toward an earlier spring in North America. Cayan *et al.* (2001) measured the timings of the first bloom of lilac and honeysuckle bushes and the first major pulse of snowmelt and found an earlier spring onset in the western United States since the late 1970s. Nemani *et al.* (2001) found a 65-day increase in the length of the FFS in the Napa/Sonoma region of California and related this phenomenon to large increases in Pacific sea surface temperature (SST) and atmospheric water vapour. Easterling (2002) also detected an earlier end of spring freeze occurrences, a later beginning of fall frost occurrences, and an increase in the length of the FFS in the United States for the period of 1948–1999. Kunkel *et al.* (2004) analysed the temporal variability of the FFS for 1895–2000 in the conterminous United States and found different trends over the period. Their results indicate that since 1980 the length of the FFS has increased by about 1 week and that the increasing trend is more prominent in western than in eastern United States.

Many studies have investigated the relationship between the variability of the length of the FFS or the beginning of spring in United States and the variability of large-scale circulations. Cayan *et al.* (2001) found a modest relationship between the onset of spring (as indicated by the timing of the first bloom of the purple common lilac) in the western United States and the Pacific North American (PNA) pattern index. Nemani

* Corresponding author: L. Yu, Applied Hydrometeorological Research Institute, Nanjing University of Information Science and Technology, Nanjing, China. E-mail: yulj@msu.edu

et al. (2001) found that the interdecadal variability of the Pacific Decadal Oscillation (PDO) may be related to an increase in the length of the FFS in the Napa and Sonoma valleys. Stewart *et al.* (2004) also noted that the change in the onset of springtime snowmelt across western North America is partly controlled by PDO. The seasonal transition of temperature and precipitation in the western United States has also been linked to the Northern Annular Mode (NAM) (Stephanie and Russell, 2008). Huntington *et al.* (2004) found that the timing of spring runoff in the New England region is correlated significantly to the North Atlantic Oscillation (NAO) and PNA.

This study focuses on the FFS in the Great Lakes region, an important agricultural production area in the United States with more than $15 billion a year in agricultural products and 7% of total US food production. The climate of the Great Lakes region is heavily influenced by the presence of the Great Lakes, which tend to moderate the magnitude and seasonality of air temperatures and enhance cloudiness, cold season precipitation, and evapotranspiration rates in areas downwind of the lakes (Changnon and Jones, 1972).

A variety of speciality crops in the Great Lakes region benefit from the temperate climate and an extended FFS along the lakeshores, especially in lee-side areas of the lakes with hilly terrain which enhances cold air drainage away from crops. In contrast to the majority of the world's major food crops in which the primary climatological production constraint is the amount and timing of precipitation during the growing season, the primary weather-related constraint for most temperate tree fruit crops is the frequency and severity of freeze events during the spring season (Flore, 1994). Tree fruits including apples, cherries, and peaches have been produced commercially in the region for more than 150 years and have a major economic impact on the region. The farm gate value of all fruit and nut crops produced in the eight US states bordering the Great Lakes typically totals more than $1 billion (USDA NASS, 2013). Meteorological conditions associated with freezing air temperature events at the surface during the transitional spring and fall seasons are consistent across the region. Most events take place during the early morning through sunrise hours and are associated a cyclonic troughing pattern across central and eastern North America at the middle and upper levels of the troposphere, a Canadian or Arctic origin anticyclone at the surface with the center located in or near the region, relatively clear skies, and a decoupling of the surface boundary layer which leads to calm winds and rapid radiational cooling of the surface (Andresen and Winkler, 2009). Climatology of the FFS for the Great Lakes region can be obtained from a climate atlas of frost-free periods and air masses (http://epa.gov/greatlakes/atlas/glatch2.html#Climate Change).

In recent decades, a noticeable increase in average temperatures in the Great Lakes region, especially in winter, has led to a longer FFS by more than 1 week, mainly due to earlier dates for the last spring frost (LSF) (Karl *et al.*, 2009). However, the frequency of spring freeze events following initial phenological development has increased during the same time frame, resulting in relatively greater risk of production losses with time (Andresen *et al.*, 2012). Spring freezes have had profound impacts on regional fruit production in recent years. An unprecedented heat wave in March 2012 brought fruit crops out of their dormant state more than 1 month earlier than normal. A subsequent series of 15–20 freeze events during April and May resulted in catastrophic freeze damage in Michigan, with tart cherry and apple yields reduced by 90 and 88% relative to the previous year's production, respectively (USDA NASS, 2013). A similar early warm up and freeze event reduced yields by more than half during the 2002 season.

Although several studies have investigated the relationship between the FFS in the western and northeastern regions of the United States and large-scale circulation patterns (Nemani *et al.*, 2001; Huntington *et al.*, 2004; Stewart *et al.*, 2004; Stephanie and Russell 2008), no studies have, to our knowledge, focused on the interannual variability of the FFS in the Great Lakes region. Owing to the dependence of agricultural activities on the FFS in the Great Lakes region, it is necessary to understand how global climate anomalies affect the FFS over the region. Hence this study will examine the spatial and temporal variability of the FFS over the Great Lakes region, with a focus on interannual variability and its relationship to global circulations. Although local, microscale factors such as topography, soils, and vegetation type may have significant influence on the timing and severity of frost events, the focus of this study will be on larger, mesoscale patterns and the link between the regional and synoptic-scale patterns because climatology of frost events at different spatial scales is likely to be highly correlated (Andresen and Winkler, 2009).

The rest of the paper is organized as follows: the data sets and methods used in the study are described in Section 2. Section 3 presents the climate and climate variability of the FFS. Section 4 gives a discussion of the data used and the results. A summary of the results and conclusions are presented in Section 5.

2. Datasets and methods

The study examines three climate variables, LSF, first fall frost (FFF), and FFS, for the region between 40°–50°N and 94°–75°W that covers the five Great Lakes and the surrounding land areas (Figure 1). The variables are calculated using the inclusive threshold of 0 °C for daily minimum temperature. It should be noted that the term 'frost' used in this article is not traditional frost and only indicates a state of air temperature below 0 °C, for the traditional frost does not apply to the lakes.

The dataset used to derive these variables is the North America Land Data Assimilation System Phase 2 (NLDAS-2) data, a long-term (1979–present) high-resolution atmosphere and land surface hydrology dataset for central North America produced by driving

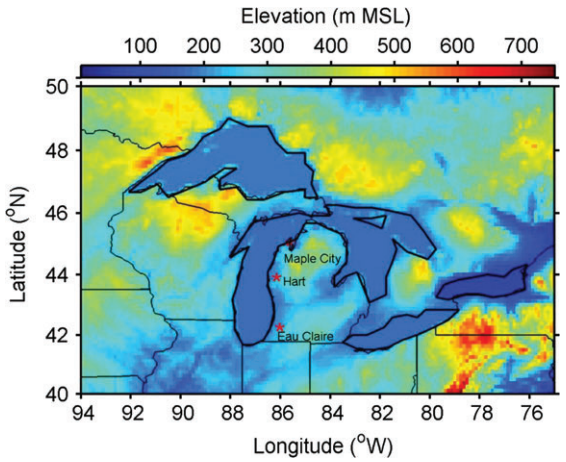

Figure 1. The topography of the study domain (40°–50°N, 94°–75°W). Three red asterisks indicate the observation sites used for comparison with NLDAS-2 data.

land surface models with a suite of observational and reanalysis products (Mitchell *et al.*, 2004). NLDAS-2 corrected the biases in precipitation and downward shortwave radiation of NLDAS-1 (Luo *et al.*, 2003; Pan *et al.*, 2003; Sheffield *et al.*, 2003; Alonge and Cosgrove, 2008). Except for precipitation and downward shortwave radiation, other forcing variables in NLDAS-2, including the 2-m temperature used in this study, come from the North American Regional Reanalysis (NARR) (Mesinger *et al.*, 2006). NLDAS-2 is chosen over NARR for its higher spatial (1/8th degree) and temporal (hourly) resolution (as compared to 32 km and 3 hourly in NARR). The study domain is shown in Figure 1 that contains 81 × 153 NLDAS-2 data points. The minimum temperature at every grid point in the study domain is computed from the 24 hourly temperatures.

A major focus of this study is to understand the connection between the interannual variability of frost dates and the length of FFS and the variations in large-scale circulation patterns. To define large-scale circulations, a global data set with both surface and upper air variables is needed and the National Centers for Environmental Prediction (NCEP) global reanalysis data (Kalnay *et al.*, 1996; Kister *et al.*, 2001) is selected for this purpose. The NCEP global reanalysis has a horizontal resolution of T62 (209 km) and 28 vertical levels, and a temporal coverage of 4 times per day from 1 January 1948 to the present. The global reanalysis used in this study is the revised version referred to as NCEP-DOE (Department of Energy) global reanalysis, which corrected errors discovered in the earlier version (Kanamitsu *et al.*, 2002). In addition to the NCEP global reanalysis, the National Oceanic and Atmospheric Administration (NOAA) extended reconstructed SST data and PDO index (Mantua *et al.*, 1997) (http://www.cdc.noaa.gov/data/gridded/data.noaa.ersst.v2.html) are also used to help define large-scale circulation patterns.

The Empirical Orthogonal Function (EOF) technique is used to identify the spatial patterns of the frost dates and FFS. The EOF analysis can produce a set of modes that consist of spatial structures (EOFs) and corresponding time series (principal components or PCs). For each mode, its EOF and PC are orthogonal to the EOFs and PCs of all other modes. Each mode has a corresponding eigenvalue that describes the variance explained by the mode. In this study, we analyse the first three modes that together explain more than 50% of the variance. The atmospheric variables are regressed onto the PCs of the first two modes to analyse the relations between large-scale circulation patterns and spatial patterns of the two leading modes. The atmospheric variables regressed to the time series of the first two EOF modes of the date of the LSF and FFF are averaged over spring (March, April, and May) and fall (September, October, and November) seasons, respectively.

3. Results and discussions

We first examine the domain-averaged values of frost dates and the length of the FFS with a focus on the interannual variability and trends. This is followed by a look at the spatial variability of the climatological means obtained by averaging values over the 31-year study period at each grid point. EOF analyses are then performed to understand the dominant spatial patterns of the interannual variability. Finally, the leading EOF modes are explained by exploring their connection to the anomalies of large-scale circulation patterns.

3.1. Interannual variability and trend

The Julian dates (JD) of LSF and FFF and the length of FFS are estimated using data from NLDAS-2 at each grid point over the study domain for every year during the 31-year study period from 1980 to 2010. The values are then averaged over all grid points to obtain domain-averaged dates of LSF and FFF and the length of FFS. The results show that when averaged across the entire Great Lakes region and over the 31-year period, the date of the LSF is 117 (April 27) and the date of FFF is 294 days (October 21), which gives an average FFS length of 177 days.

The time series and trends of domain-averaged LSF, FFF, and FFS are shown in Figure 2. All three exhibit considerable interannual variability. During the period of 1980–2010, the earliest LSF occurred on 16 April 1998 whereas the latest LSF was on 8 May 1996, a 23-day difference. The difference between the earliest and latest FFF is also 21 days. The large interannual variability of the dates of FFF and LSF results in large variability of the FFS with the longest FFS of 198 days occurring in 1998 and the shortest of 159 days in 1996.

Upon examining the spectral characteristics of the time series in Figure 2, the interannual variation of the date of FFF and the length of FFS exhibit a 3.5-year period and the date of LSF has a shorter period of 2.5 years (not shown). The 2.5-year period for the date of LSF may be

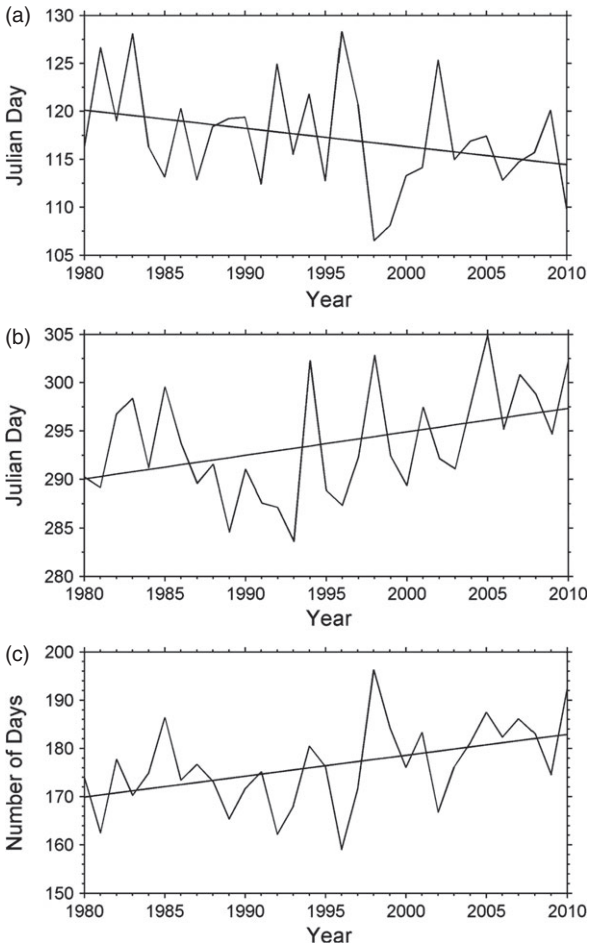

Figure 2. Time series and trends of domain-averaged dates of the last spring frost (a), the first fall frost (b), and length of the frost-free season (c) during the period of 1980–2010.

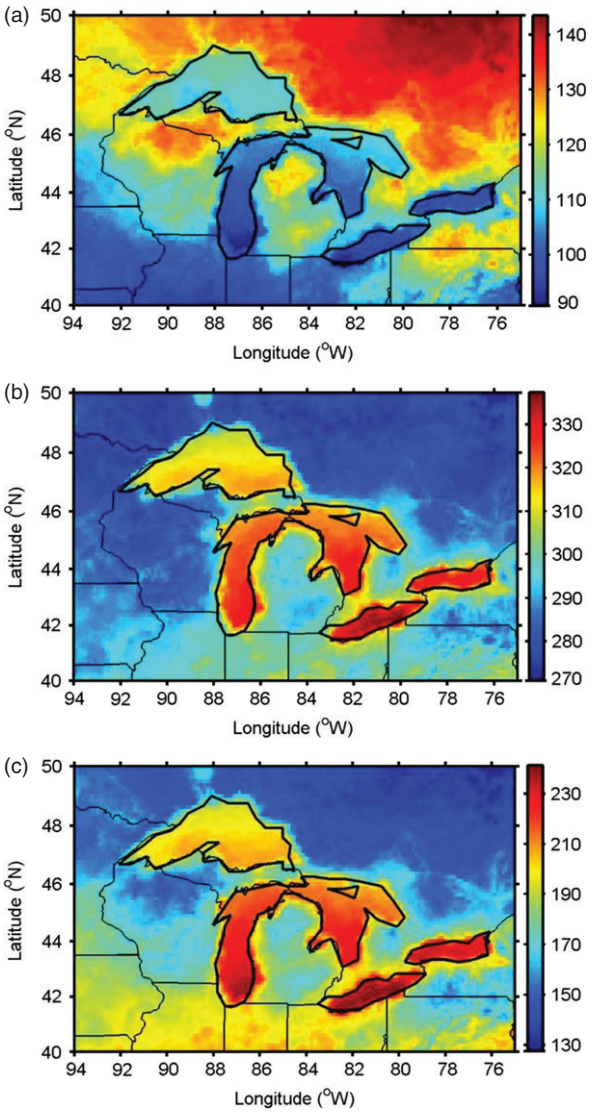

Figure 3. Climatologies of the date of the last spring frost (a), the date of the first fall frost (b), and the length of the frost-free season (c) during the period of 1980–2010. (Unit: day).

related to the NAO (Schneider and Schonwiese, 1989; Cook *et al.*, 1998; Higuchi *et al.*, 1999).

A linear trend is estimated by applying least squares regression to the time series in Figure 2. The date of LSF shows a decreasing trend of -0.19 day year^{-1}, implying an earlier beginning of spring in the 2000s than in the 1980s. The date of FFF exhibits an increasing trend at 0.24 day year^{-1}, implying a later start of fall frost. The combination of an earlier start of spring and later onset of fall frost leads to an increasing trend of 0.43 day year^{-1} for FFS during the 1980–2010 period. Relative to the earlier beginning of spring, the later start of fall makes the larger contribution to the lengthening of FFS.

3.2. Spatial variability

The spatial distributions of the dates of LSF and FFF and the length of FFS across the Great Lakes region averaged over the 31-year study period are shown in Figure 3. The spatial pattern of the climatological dates for LSF is characterized by an increase from southwest to northeast across the region and an increase from the lake surfaces to the surrounding land. The earliest LSF (91 JD) occurs over the southern end of Lake Michigan and Lake Erie, whereas the latest (144 JD) is seen over southern Quebec. The climatological minimum temperature in spring (not shown) exhibits a spatial pattern that is opposite to that of the date of LSF, suggesting that higher minimum temperatures in spring correspond to earlier occurrences of LSF.

The spatial pattern of the climatological dates of FFF shows a reversed trend from that of LSF, with delayed occurrence moving from North to South and from land to water (Figure 3(b)). The latest FFF of 337 JD occurs over Lake Erie. During the spring and fall seasons, due to the larger heat capacity of water, the nighttime temperatures over the lake surfaces are warmer than temperatures over surrounding land areas, thus decreasing the occurrence of frost over lakes. Scott and Huff (1997) investigated the effects of the Great Lakes on the average minimum temperature and found 3–4 °C higher surface temperature over Great Lakes than surrounding land in spring and fall.

The combined effect of the earlier LSF and later FFF lengthens the FFS over the Great Lakes with the longest FFS of 241 days occurring over Lake Erie. The shortest FFS of 128 days occurs in southern Quebec. Overall, the patterns are very similar to results obtained in previous studies with single site observation series (Eichenlaub *et al.*, 1990; MRCC, 2013).

At any given location, the dates of LSF and FFF and the length of FFS may vary significantly from year to year. The interannual variability of these variables at each location is estimated by computing their standard deviations. The variables at each location are first de-trended before standard deviations are computed. The spatial distribution of the standard deviations across the region is shown in Figure 4. The standard deviation for FFS varied from 6 to 23 days, which is comparable to the range of the standard deviation for FFF (7–27 days). The standard deviations are larger over the lakes (Lake Michigan, Lake Ontario and Lake Huron) and smaller in the northern portion of the region for both FFS and FFF. For LSF, the standard deviation is smaller over the lakes and in the northeastern and southwestern portions of the region compared to the rest of the region.

As shown in Figure 3, there are large differences between the values of all three variables over land and over the Great Lakes. Land-averaged values of the three variables are influenced mainly by large-scale circulations, and the values over the Great Lakes are regulated not only by large-scale circulations but also by the heat of the Great Lakes. To explore the relationship between the land-averaged and lake-averaged values of the three variables, correlation coefficients between the land-averaged values and lake-averaged values are calculated for the five lakes and the results are shown in Table 1. For the date of LSF, the relationship between land-averaged and lake-averaged values is significant at above 99% confidence level for all five lakes. The correlation is weaker for FFF compared to LSF, suggesting that FFF is more sensitive to the lake effect. The reason for this difference may be that the lake effect on minimum temperature is larger in the fall than in the spring (Figures 7 and 11; Scott and Huff, 1997). The interannual variability of the length of FFS is also mainly controlled by the variability of large-scale circulations.

The trends shown in Figure 2 are domain-averaged values of LSF, FFF, and FFS. As the average can mask regional differences, the spatial variability of the trends is shown in Figure 5 for the entire region. The trends for LSF are, in general, negative over much of the region except for the northwest, the southwest, and small areas southeast of Lake Erie and southern Quebec where weak positive trends are found. All lakes and their shores exhibit negative trends and the largest negative trend of -1.1 day year^{-1} is found over western Lake Superior. An examination of the springtime daily minimum temperature reveals an increasing trend across most of the Great Lakes region (Figure 6(a)). Meanwhile the number of days with springtime minimum temperature below freezing exhibits a decreasing trend over the region (Figure 6(c)).

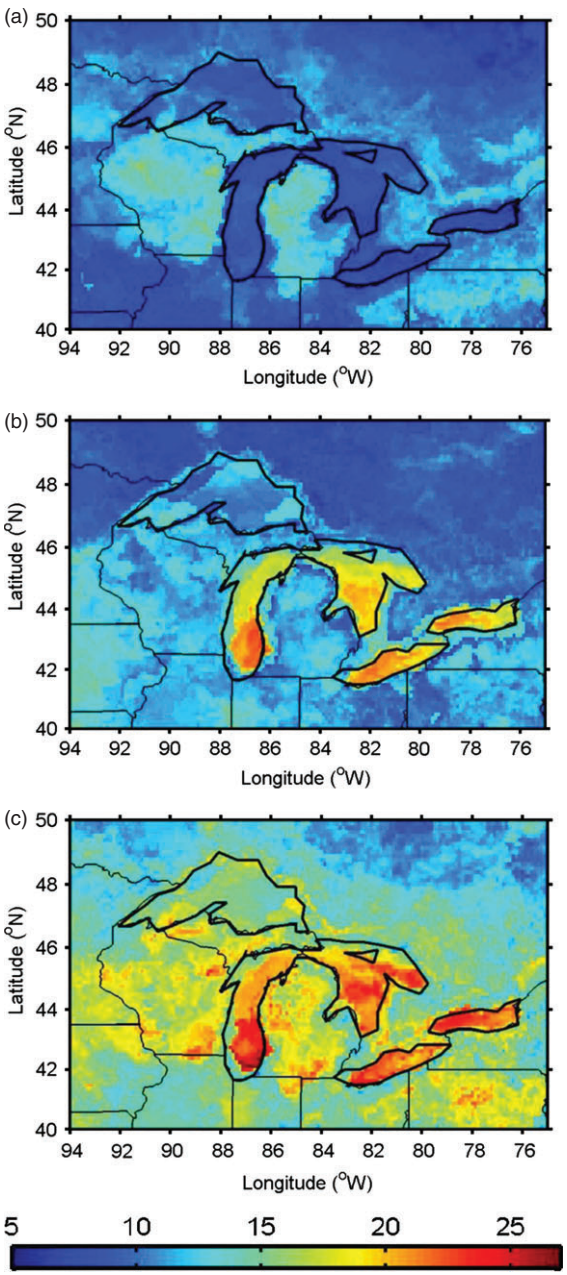

Figure 4. Interannual standard deviations of the date of the last spring frost (a), the date of the first fall frost (b), and the length of the frost-free season (c) during the period of 1980–2010. (Unit: day).

A comparison between land-averaged and lake-averaged trends (Table 2) reveals a much larger trend over all five lakes than over land. The land-averaged trend for LSF is -0.14 day year^{-1}. Among the five lakes, Lake Michigan and Lake Superior have the largest negative trend of -0.53 and -0.52 day year^{-1}, respectively, and Lake Erie has the smallest negative trend of -0.44 day year^{-1}.

In contrast to the trends for LSF, positive trends for the date of FFF are seen across most of the Great Lakes region except for the western and southwestern sections.

Table 1. Correlations between land-averaged and lake-averaged dates for the last spring frost and the first fall frost and the length of frost-free season over the Great Lakes region during the period of 1980–2010.

The Great Lakes	Superior	Michigan	Huron	Erie	Ontario
The date of LSF	0.72***	0.63***	0.67***	0.66***	0.46***
The date of FFF	0.48***	0.39*	0.44**	0.29	0.35
The length of FFS	0.64***	0.65***	0.62***	0.57***	0.58***

One, two, and three asterisks indicate above 95, 98, and 99% confidence level, respectively.

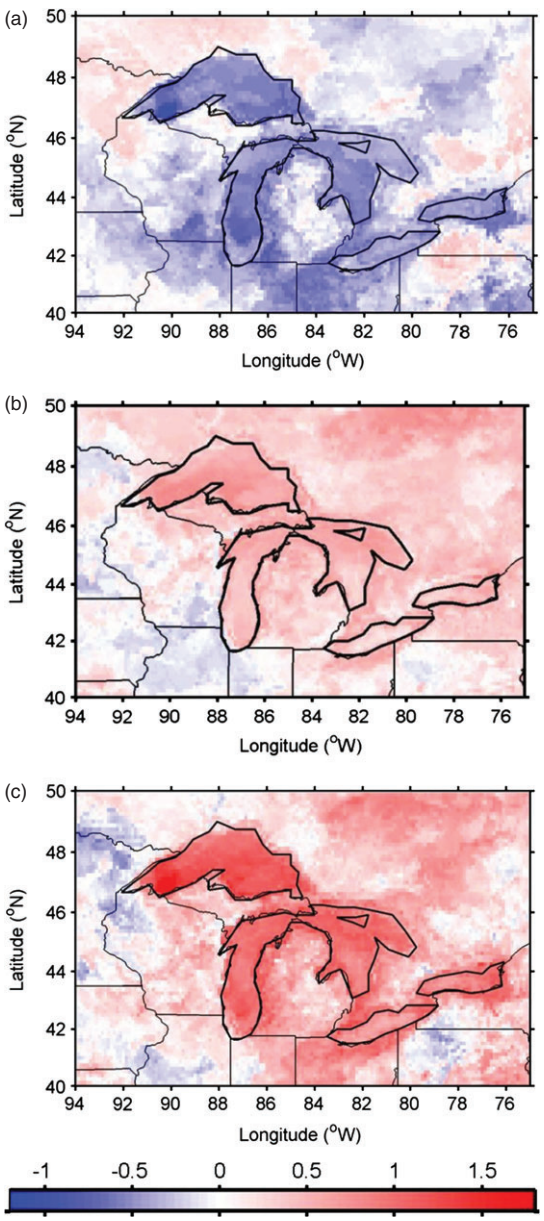

Figure 5. Trends in the date of the last spring frost (a), the date of the first fall frost (b), and the length of the frost-free season (c) during the period of 1980–2010. (Unit: day year^{-1}).

The sharpest positive trend of 0.83 day year^{-1} is found over western Lake Superior and the largest negative trend of −0.49 day year^{-1} is seen at the western boundary in southeastern Minnesota. The minimum temperature in the fall season shows an increasing trend over the entire Great Lakes region (Figure 6(b)), whereas the number of days with minimum temperatures below freezing in the fall exhibits a decreasing trend (Figure 6(d)). These changes in minimum temperature may result in a later date of FFF over the Great Lakes region. Similar to LSF, the trends over the lakes that range from 0.35 for Lake Erie to 0.55 for Lake Superior are larger than the land-averaged trend of 0.20 day year^{-1} (Table 2).

The combination of negative trends in the date of LSF and positive trends in the date of FFF yields an overall positive trend in the FFS over the Great Lakes region. Negative trends occur only in small patches of northwestern, southwestern, and southeastern sections. Similar to FFF, the largest positive trend is found over Lake Superior and the weakest over Lake Erie. In the next section, an explanation for the trends is given in the context of large-scale circulations.

3.3. Results of EOF analysis

EOF analyses were performed to identify the dominant spatial patterns of interannual variability of LSF, FFF, and FFS across the Great Lakes region. Below, we discuss the results of the EOF analyses and the relation between the leading EOF modes and the variation of large-scale circulations for each of the three variables individually.

3.3.1. The last spring frost

The leading two modes of the date of LSF are shown in Figure 7. The first mode explains 29.91% of the total variance, and the fluctuation is in phase everywhere in the domain except for a small area northeastern of Lake Erie (Figure 7(a)). Large variability occurs over Michigan and Wisconsin, and small variability appears in the Canadian provinces bordering the Great Lakes to the north and northeast and along the southern border of the region especially southwest. The spatial pattern of the first EOF mode is similar to that of interannual standard deviation (Figure 4(a)). The EOF time series or the expansion coefficients of the first EOF mode show a strong interannual variability and the spectral analysis of the time series (not shown) reveals major periods of 2.5 and 4 year.

The second mode accounts for only 11.68% of the total variance. The variability appears to be out of phase across the region with positive values over the lakes, along the southern border, in the southwest and northeast, and negative values in the rest of the region (Figure 7(c)). The spatial pattern of the second mode appears to be opposite

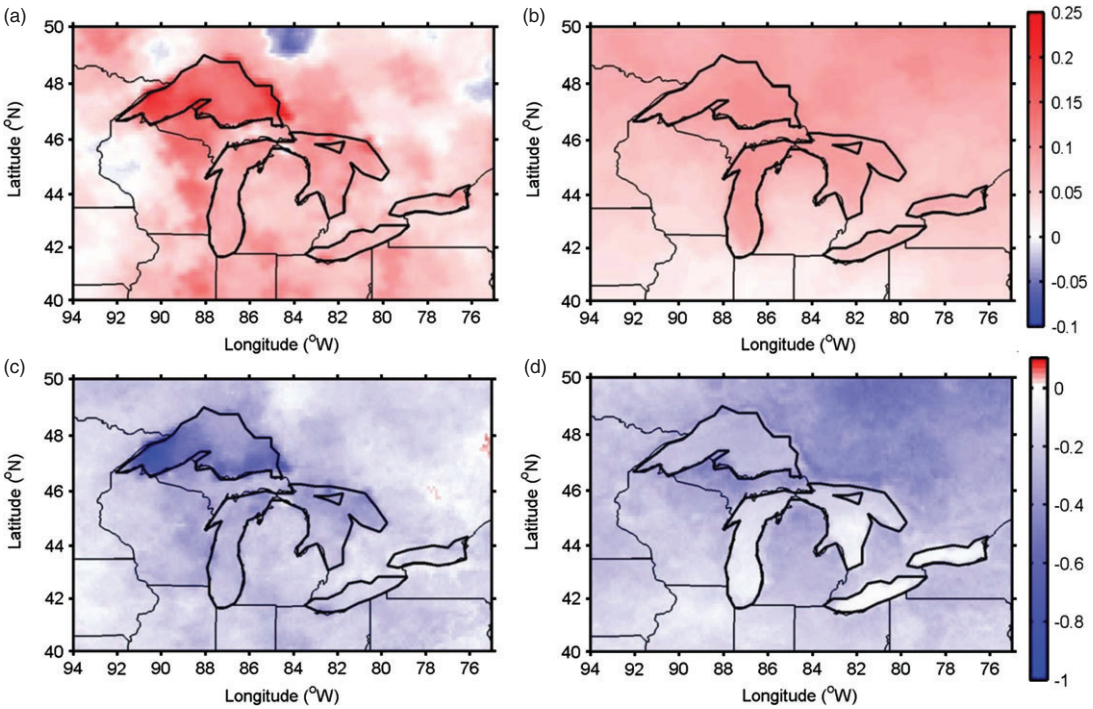

Figure 6. Trends in minimum temperature in spring (a) and fall (b) (K year^{-1}) and the number of days with minimum temperature <273 K in spring (c), and fall (d) (year^{-1}) during the period of 1980–2010.

Table 2. Trends in the dates of the last spring frost and the first fall frost and the length of frost-free season over the land areas and over the five lakes of the Great Lakes region during the period of 1980–2010 (Unit: day year^{-1}).

	Land	Superior	Michigan	Huron	Erie	Ontario
The date of LSF	−0.14	−0.52	−0.53	−0.46	−0.44	−0.45
The date of FFF	0.20	0.55	0.44	0.49	0.35	0.41
The length of FFS	0.34	1.07	0.97	0.95	0.79	0.86

to the pattern of topography (Figure 1), with later dates of LSF associated with lower terrain and earlier dates of LSF occurring over higher elevations. But the regions with low (high) elevations have a decreasing (increasing) trend in the date of LSF. Figure 7(c) also reflects the different effect of Great Lakes and land on the date of LSF.

To quantitatively understand the spatial patterns of the leading two EOF modes of the date of LSF in the context of atmospheric circulation anomalies, the time series of the first two EOF modes are regressed to spring season mean atmospheric variables, including the 200 hPa geopotential height (H200), 850 hPa wind, mean sea level pressure (MSLP), surface air temperature, and oceanic variable (SST). The results of the analyses are shown in Figure 8.

For the positive phase of the first EOF mode, a negative PNA Rossby wave train occurs over North Pacific Ocean, North America, and North Atlantic Ocean (Figure 8(a) and (b)). A positive H200 anomalous centre occurs over central tropical Pacific Ocean, Aleutian Islands, and northwestern Atlantic Ocean. Negative H200 anomalies occupy mid-latitude North Pacific Ocean and most of Canada and the United States. Owing to an equivalent barotropic structure of the wave train, MSLP anomalies north of 25°N are similar to that of H200. The wave train weakens the Aleutian Low and strengthens the trough over North America, which helps bring cold air southward into the Great Lakes region. The negative H200 and MSLP anomalies over northeastern Canada, Greenland, and Iceland and positive anomalies over central North Atlantic Ocean are characteristics of the positive NAO. A baroclinic structure with an opposite variation tendency between MSLP and H200 occurs over tropical central Pacific Ocean, where a positive SST excites negative MSLP and positive H200 anomalies, which is the source for the Rossby wave train. A negative SST anomaly over the central North Pacific Ocean and a positive SST anomaly over the northeastern Pacific Ocean also reinforce the wave train by local ocean–atmosphere interactions. The spatial pattern of anomalous SST-regressed time series of the first mode shows a similar structure to a developing El Niño pattern (Figure 8(c)).

Under the influence of the anomalous trough over North America, an anomalous northwesterly flow from the Arctic advects cold and dry air into North America, lowering surface temperatures over most of the North

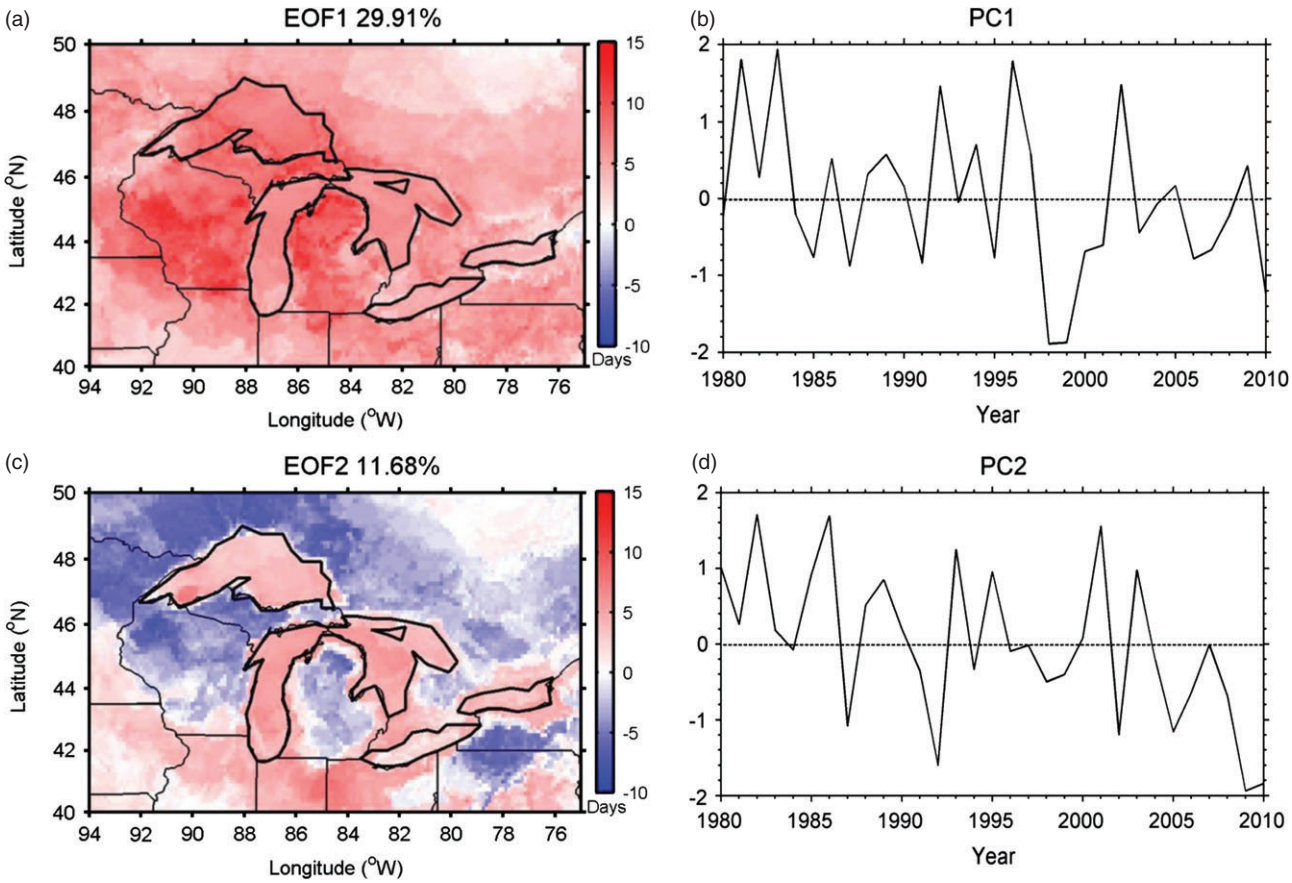

Figure 7. Spatial patterns (a) and (c) and the time series of the coefficients (b) and (d) of the first two leading EOF modes of the date of the last spring frost for the period of 1980–2010: (a) and (b) the first mode, (c) and (d) the second mode.

American continent (Figure 8(d) and (e)). In the Great Lakes region, this Arctic air intrusion produces large negative surface temperature anomalies of more than 0.5 °C over most of the region. The decrease in springtime surface temperature is in favour of the formation of springtime frost and the delay of the date of LSF over the Great Lakes region.

During the negative phase of the first mode, a positive Rossby wave is excited by a negative SST anomaly over tropical central Pacific Ocean. An opposite anomalous circulation over North America increases springtime surface temperature and delays the onset of LSF over Great Lakes region. The onset of spring in the western United States is related to the springtime PNA index with a correlation coefficient of 0.41(Cayan *et al.*, 2001). These correlations are modest because PNA is mostly a wintertime atmospheric teleconnection pattern (Wallace and Gutzler, 1981) and its amplitude diminishes and location changes during the spring season (Barnston and Livezey, 1987). Another possibility is that apart from oceanic processes, terrestrial processes may influence the PNA pattern (Cayan *et al.*, 2001).

Similar regression analyses are also performed for the second EOF mode and the results are shown in Figure 9. A Rossby wave train, imbedded within the westerly jet stream, occurs over the central Pacific Ocean and North America (Figure 9(a)). The wave train is similar to the circumglobal teleconnection (CGT) in the Northern Hemisphere summer (Ding and Wang, 2005), which is associated with the Indian summer monsoon and the jet exit region over the North Atlantic Ocean. Under the influence of this wave train, the Great Lakes region is affected by a negative H200 anomaly, which is accompanied by an anomalous cyclonic circulation at 850 hPa (Figure 9(b)). The cyclonic circulation brings cold and dry air into the Great Lakes region (not shown). Wang *et al.* (2012) found that there is substantial ice cover over the Great Lakes in the spring season, especially in March over Lakes Superior and Huron. Hence the decrease in surface temperature also postpones the melting of Great Lakes ice and the date of LSF. The westerly wind also decreases surface temperature of the southern Great Lakes through enhanced mixing and evaporation.

3.3.2. *The first fall frost*

Similar to LSF, the first EOF mode for the date of FFF accounts for 29.03% of the total variance and the second mode accounts for 12%. The spatial patterns and the time coefficients for the first two modes for FFF are shown in Figure 10. The variability is in phase across the region except for a small patch to the northwest of Lake Superior. Large variability occurs over areas in the southeast

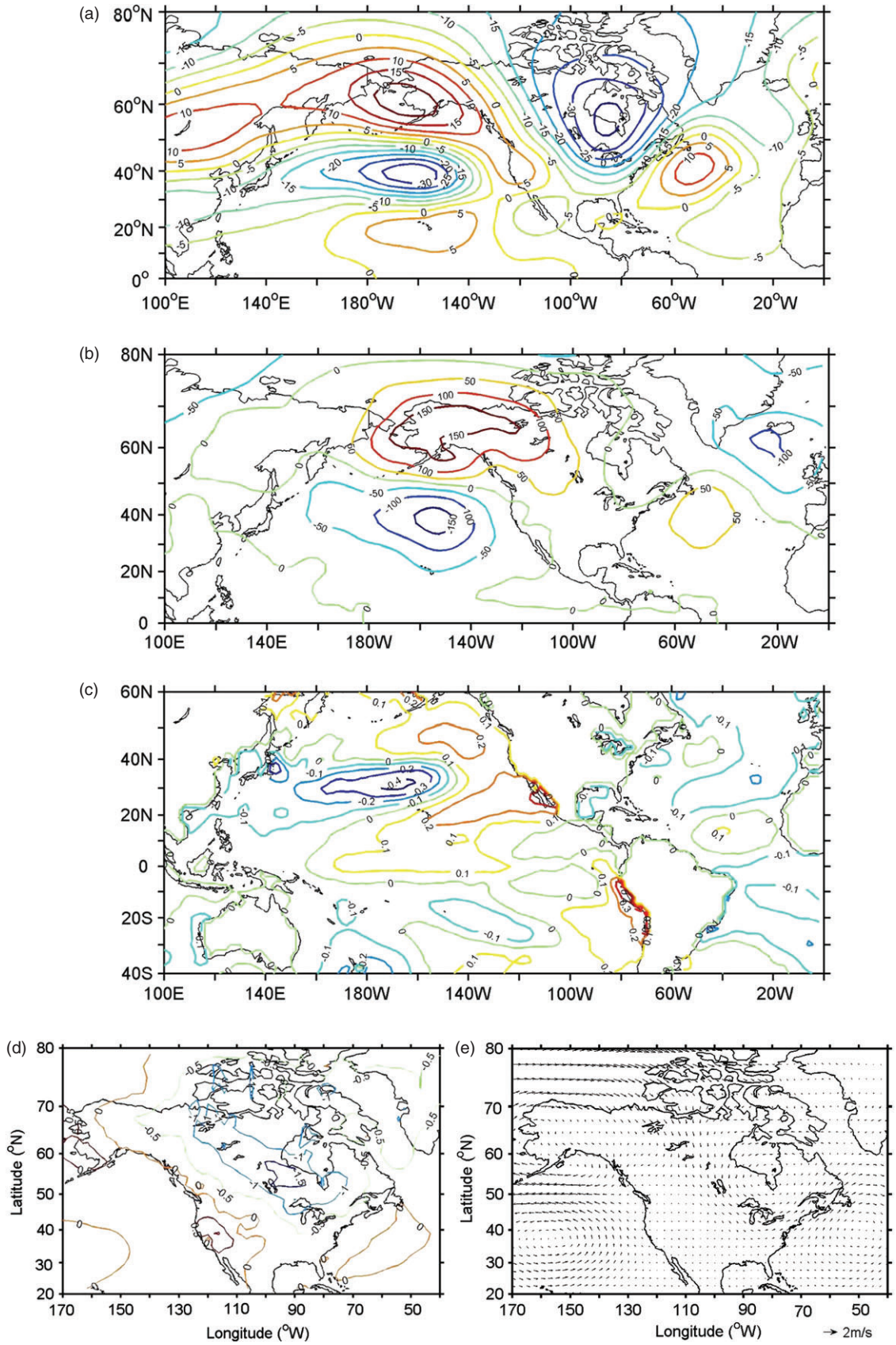

Figure 8. The anomalous (a) 200 hPa geopotential height (gpm), (b) mean sea level pressure (Pa), (c) sea surface temperature (°C), (d) surface temperature (°C), and (e) 850 hPa wind ($m\,s^{-1}$) maps regressed to the time series of the first EOF mode of the date of the last spring frost for the period of 1980–2010.

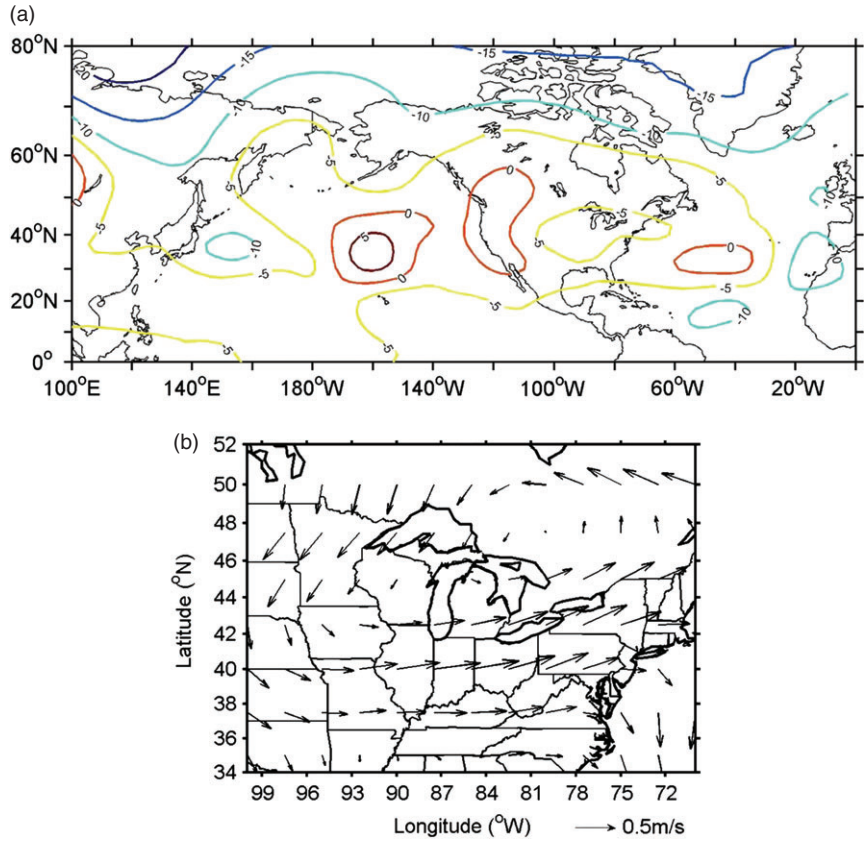

Figure 9. The anomalous (a) 200 hPa geopotential height (gpm) and (b) 850 hPa wind ($m\,s^{-1}$) maps regressed to the time series of the second EOF mode of the date of the last spring frost for the period of 1980–2010.

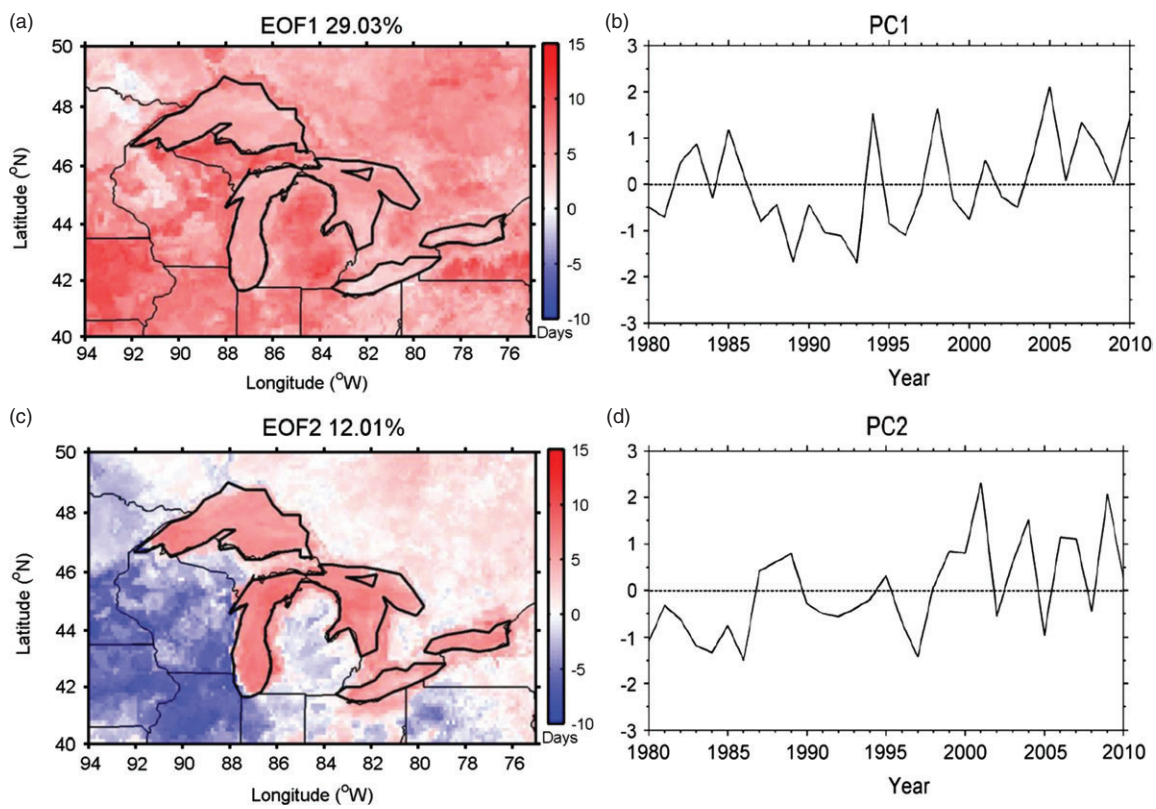

Figure 10. Spatial patterns (a) and (c) and the time series of the coefficients (b) and (d) of the first two leading EOF modes of the date of the first fall frost for the period of 1980–2010: (a) and (b) the first mode, (c) and (d) the second mode.

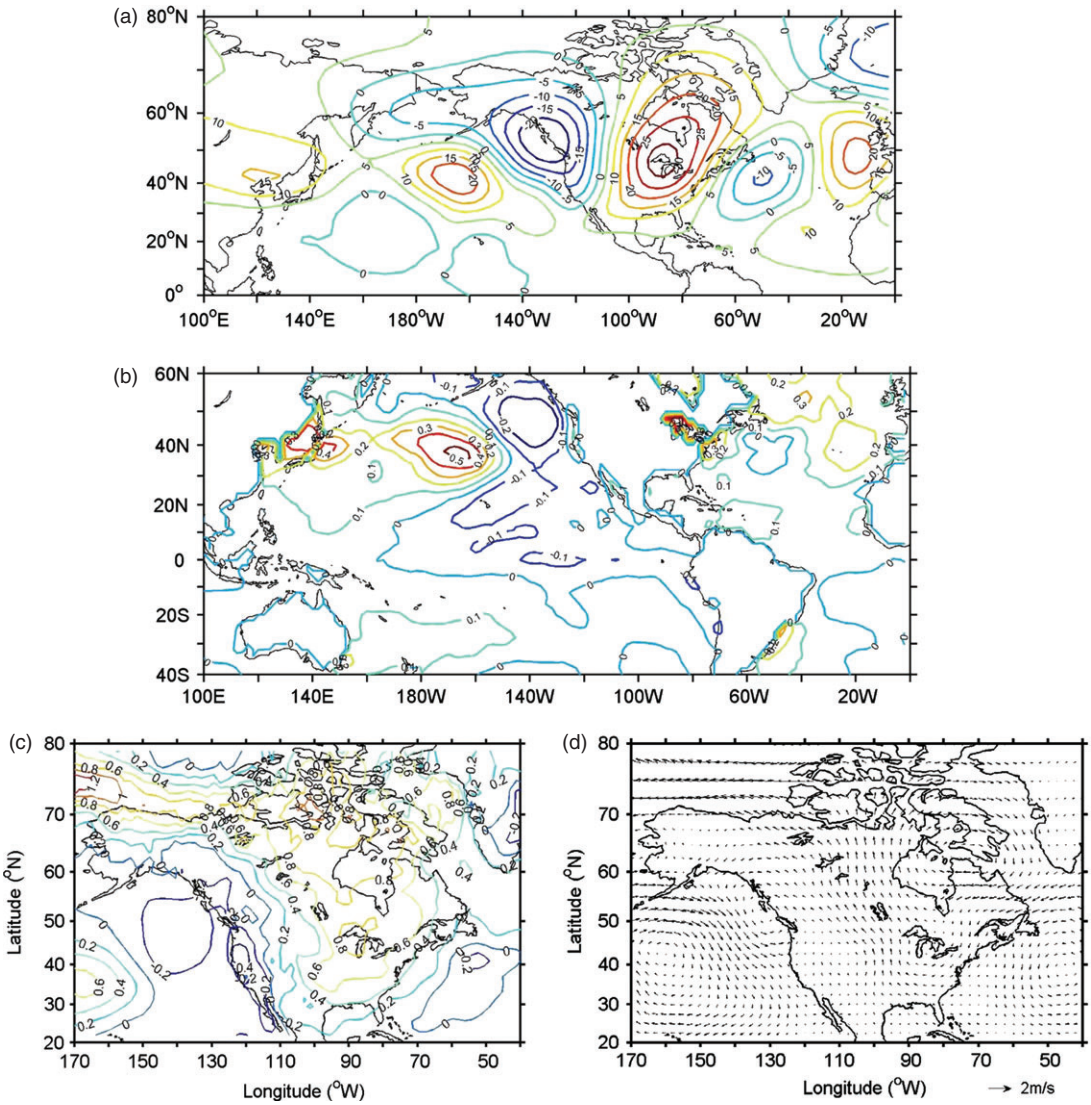

Figure 11. The anomalous (a) 200 hPa geopotential height (gpm), (b) sea surface temperature (°C), (c) surface temperature (°C), and (d) 850 hPa wind ($m\,s^{-1}$) maps regressed to the time series of the first EOF mode of the date of the first fall frost for the period of 1980–2010.

and southwest of the region and areas south of Lake Superior and east of Lake Michigan. The main period of variation, as revealed by the spectral analysis of the time series (not shown), is 3.5 years. The spatial pattern of the second mode shows an out-of-phase variability with positive anomalies over the lakes and in the Canadian Great Lakes provinces and negative anomalies across the rest of the region. Similar to LSF, the large positive anomalies occur over the Great Lakes (Figure 10(c)). The major period of the second time coefficient is 3 years. Both the first and second modes are associated with PDO, with fall season correlation coefficients of −0.48 and −0.42 between the first and second coefficient and the PDO indices.

Similar regression analyses are also applied to the date of the FFF and the results are shown in Figure 11. A Rossby wave train originates over the tropical western Pacific Ocean extending northeastward into western Canada and southeastward into the United States, North Atlantic Ocean, and Europe (Figure 11(a)). The positive H200 anomalous centres occur over the central North Pacific Ocean (40°N, 160°W), the Great Lakes region, and the eastern North Atlantic Ocean (50°N, 20°W). The negative H200 anomalous centres occur over the tropical western Pacific Ocean (20°N, 170°W), western Canada (50°N, 130°W), and the western North Atlantic Ocean (40°N, 50°W). The spatial pattern of anomalous SST over the Pacific Ocean shows a PDO cool phase over mid and high latitudes (Zhang *et al.*, 1997) (Figure 11(b)). In addition, the lake surface temperatures over the Great Lakes and SST over the North Atlantic Ocean and Japan Sea show positive anomalies whereas a negative SST anomaly occurs over the western North Atlantic Ocean. The positive (negative) H200 anomalies correspond to the positive (negative) sea or lake surface temperature anomalies.

Compared with Figure 8(a), the positive H200 anomaly over North America in Figure 11(a) weakens the trough over North America and associated Arctic cold air

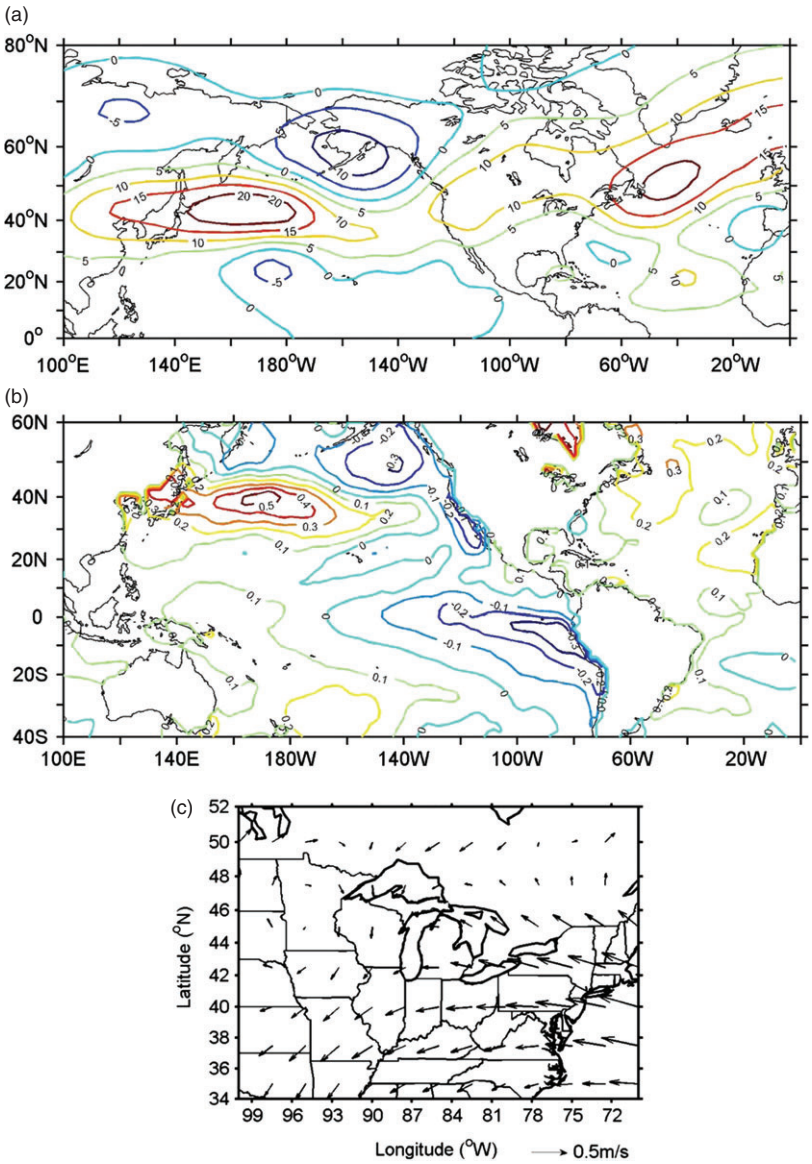

Figure 12. The anomalous (a) 200 hPa geopotential height (gpm), (b) SST (°C), and (c) 850 hPa wind ($m\,s^{-1}$) maps regressed to the time series of the second EOF mode of the date of the first fall frost for the period of 1980–2010.

invasions, leading to positive surface temperature anomalies over most of North America. The positive H200 anomaly over the Great Lakes region and the southeasterly wind on the western side of the anticyclone increase surface temperatures by 0.8 °C over the western Great Lakes region. The positive H200 anomaly and the northeasterly wind on the eastern side of the anticyclonic circulation lead to an increase in surface temperature of more than 0.6 °C over the eastern Great Lakes region.

Figure 12 shows the regression map of atmospheric and oceanic variables to the second time coefficient. A Rossby wave train is excited over the subtropical central Pacific Ocean and extends from the North Pacific Ocean to the North Atlantic Ocean with positive H200 anomalies over most of North America. In contrast to Figure 11(a) and (b), the positive SST and H200 anomalies over the North Pacific Ocean are positioned more westward. It has been indicated that the SST over the Kuroshio Extension (KE) can strengthen the wave train and influence the climate in North America. Peng *et al.* (1997) and Peng and Whitaker (1999) investigated the atmospheric response to SST anomalies over KE using a general circulation model and the response dependence on background wind field and found a similar wave train. Over the tropical Pacific Ocean a typical La Niña pattern does develop, though negative SST anomalies occur over the tropical eastern Pacific Ocean. Northerly winds induced by a cyclone prevail over the western part of the Great Lakes region and easterly and southeasterly winds from Atlantic Ocean occur over the eastern part of the region. The dry and cold air results in the early date of FFF over the southwestern Great Lakes region. On the contrary, the warm and moist air leads to the delay of FFF over Great Lakes and eastern

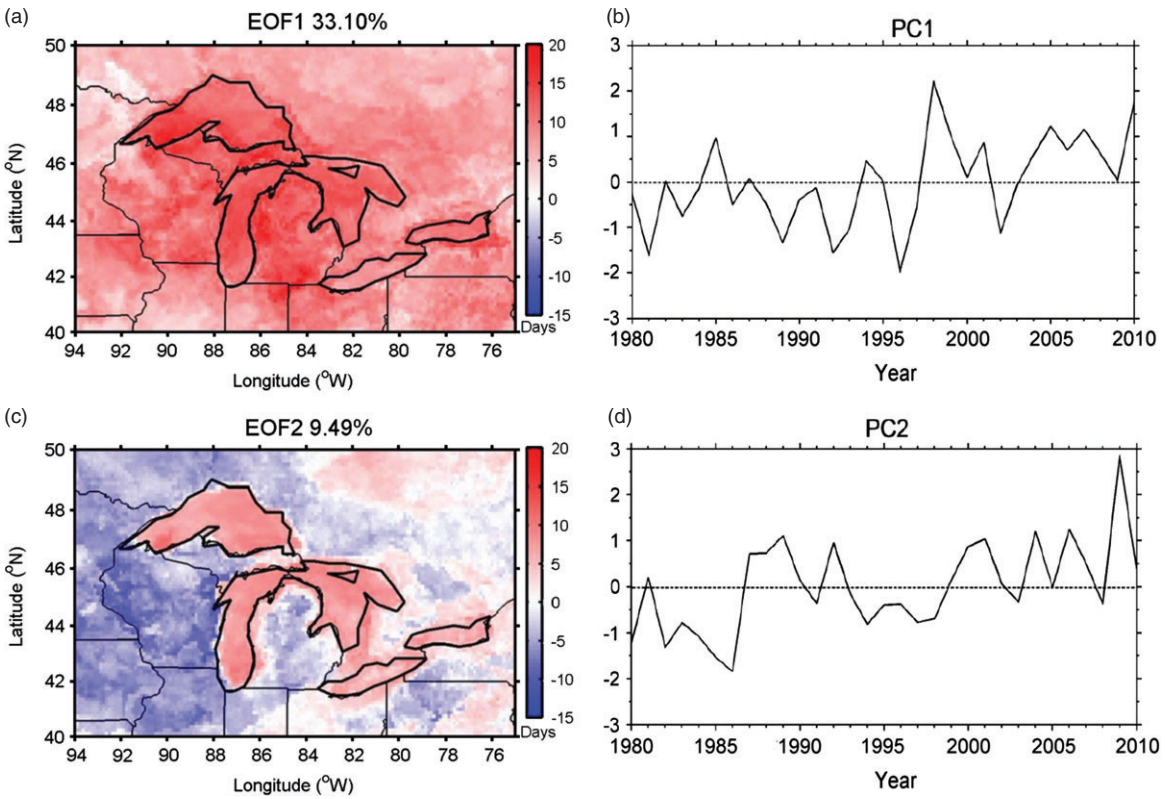

Figure 13. Spatial patterns (a) and (c) and the time series of the coefficients (b) and (d) of the first two leading EOF modes of the length of the frost-free season for the period of 1980–2010: (a) and (b) the first mode, (c) and (d) the second mode.

Great Lakes region. The large heat capacity of lake water increases the minimum surface temperature over Great Lakes and further delays the date of FFF over the Great Lakes.

3.3.3. The frost-free season

The spatial patterns and time series of the leading two modes of the length of FFS are shown in Figure 13. The first mode explains 33.10% of the total variance, which is larger than the fraction explained by the first mode for LSF and FFF. The variability is in phase across most of the region except for a small portion in the northwestern part of the domain. Large variability occurs over southwestern Lake Superior and the northern and eastern shores of Lake Michigan. The time series of the first mode reveals an interdecadal variability (Figure 13(b)).On the basis of the Mann–Kendall (MK) (Mann, 1945) abrupt change test, an abrupt change point occurred in 1997/1998, with longer FFS over most of the region after 1997/1998 and a shorter season prior to that. The first mode is significantly related to PDO, with correlation coefficients ranging from −0.39 in May to −0.60 in November. Apart from the interdecadal variability, the first time coefficient has a 3.5-year period interannual variability identified by spectral analysis (not shown).

The second mode explains only 9.49% of the total variance. An opposite phase occurs between the Great Lakes and the areas east of lakes and the western part of the region (Figure 13(c)). The spatial pattern of the second mode is similar to the spatial pattern of the trend for FFS (Figure 5(c)). The second time coefficient also displays an increasing trend. Besides the increasing trend, the major periods of the second time coefficient are 2.5–2.9 and 4.1 years. Unlike the first mode, the second time coefficient is significantly related to the PDO indices only in March and April with the correlations of −0.49 and −0.40.

The regression maps of spring and fall atmospheric and oceanic variables to the time coefficients of the length of FFS are similar to those of the time coefficients for the dates of LSF and FFF. Similar mechanisms can be invoked to explain the leading modes for FFS.

4. Discussions

The results presented above are derived from gridded reanalysis data, which is a model simulation of the past that includes assimilation of historical observations. There are pros and cons of using gridded data as opposed to station observations for this and other similar climate analyses. The major advantage is more consistent data coverage in space and time, allowing for better description of spatial patterns. The gridded reanalysis, however, is not real observations. The major caveat for this study is the potential bias in the minimum temperature which has a direct effect on the results. To examine the potential biases in the minimum temperature in the NLDAS-2 data, we obtained long-term climate records

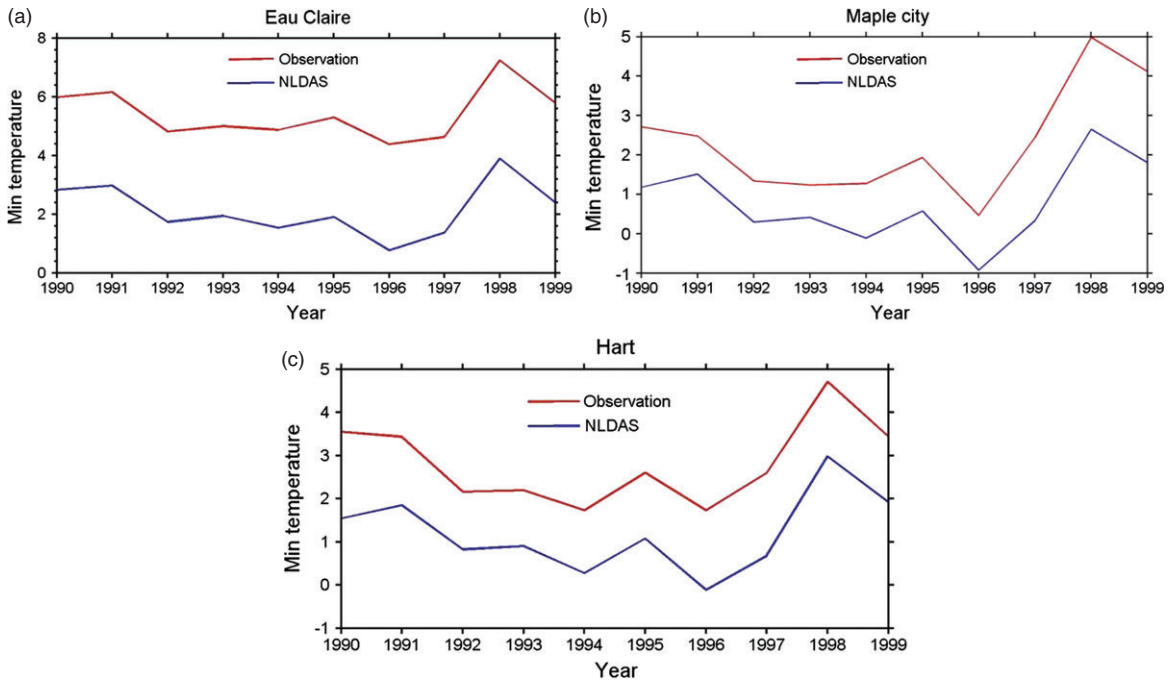

Figure 14. Comparison of annual minimum temperature between observation and NLDAS at three sites. The locations of three sites are shown in Figure 1.

from three climate stations in Michigan (locations shown in Figure 1) and compared with the NLDAS-2 minimum temperatures. The results for annual mean minimum temperature comparison at the three sites are shown in Figure 14. There appears to be a cold bias in NLDAS-2 minimum temperature. The cold bias, which has a magnitude similar to other model or gridded data products (1–3 °C), is consistent at all three locations and for all years. The existence of a cold bias implies a delay in the LSF, an earlier onset of the FFF, and a shorter FFS in the analysis compared to reality, which should be taken into consideration when assessing the climatology of these variables. The cold bias, on the other hand, has little effect on the analysis of the interannual variability (the focus of the paper); the data capture the interannual variability of the minimum temperature (with correlation coefficients of 0.9824, 0.9392, and 0.9669 for Eau Clarie, Mapple City, and Hart). This gives confidence in the results on interannual standard deviations, trends, EOF analysis of interannual variability, and the relationship with large-scale circulation anamolies.

5. Summary

In this study, temporal and spatial variability of the date of LSF, the date of FFF, and the length of FFS in the Great Lakes region for the period of 1980–2010 are investigated using two reanalysis datasets.

The domain-averaged LSF, FFF, and FFS all show strong interannual variability. The major period for the date of LSF and FFS is 3.5 years, which appears to be related to El Niño-Southern Oscillation (ENSO). The date for FFF exhibits a 2.5-year period of variation and it seems to be associated with NAO. There is a decreasing trend of -0.19 day year^{-1} for the date of LSF, an increasing trend of 0.24 day year^{-1} for the date of FFF, and a significant increasing trend of 0.43 day year^{-1} for the length of FFS during the period of 1980–2010. In other words, the trends during the past 31 years for the region as a whole suggest an earlier occurrence of the LSF, a delayed occurrence of FFF, and a lengthening of the frost-free period.

The climatology, interannual standard deviations, and trends of the three variables exhibit significant spatial variability across the Great Lakes region. Compared to the surrounding land areas, the Great Lakes have earlier LSF, later FFF, and longer FFS, but weaker interannual variability. Large-scale atmospheric circulations are shown to have more influence on LSF than FFF over the Great Lakes. The Great Lakes and their shores have a significantly negative trend for LSF and a significantly positive trend for FFF and FFS. The trends over the Great Lakes depend on the locations and depths of the lakes and the season. Collectively, the trends toward a longer FFS should potentially be beneficial to most annual crops produced in the region. The implications for perennial crops such as tree fruit are more complicated, however, as their vulnerability also depends on the phenological stage at the time of the freeze. So even though the LSF are coming increasingly earlier in the year, so are the rates of initial development. There is recent evidence that the vulnerability of fruit crops to frost damage may have even increased with time as a result of these trends (Winkler *et al.*, 2013).

EOF analyses show that the predominant modes for LSF, FFF, and FFS account for 29.91, 29.03, and 33.10% of the total variance, and they are in phase across most of the Great Lakes region. However, the second mode, which accounts for 11.68, 12.01 and 9.49% of the total variance for LSF, FFF, and FFS, mainly shows an out-of-phase variability between the Great Lakes and the land areas.

The regression analyses show that the first EOF mode for the date of LSF is mainly connected to PNA and ENSO. The positive SST anomaly over the tropical central Pacific Ocean during El Niño excites a Rossby wave train (negative PNA), which strengthens a trough over North America. A strong northwesterly wind anomaly associated with the trough advects cold and dry Arctic air into the Great Lakes region, decreasing surface temperatures, and retarding the onset of LSF. The situation is reversed during positive PNA and La Niña. The first EOF mode for FFF is related to PDO. The positive SST anomaly over the tropical central Pacific Ocean associated with a PDO cool phase also excites a Rossby wave train, where a positive 200 hPa geopotential height anomaly is over the Great Lakes region and deters the southward invasion of cold air, thus delaying the onset of the FFF; the opposite occurs during the PDO warm phase. For FFS, the first EOF mode is associated with a PDO cool phase with an abrupt change point in 1997/1998. Similar Rossby wave trains are excited in spring and fall and the same mechanisms as for FFF are applied to the regression map.

The second EOF mode for LSF is related to springtime CGT. An 850 hPa cyclonic circulation postpones the melt of the ice of the Great Lakes and decreases the surface temperature of the Lakes by mixing and evaporation. The second EOF mode for FFF is associated with PDO, which triggers a Rossby wave train over the North Pacific Ocean, North America, and North Atlantic Ocean. Local wind fields induced by the wave train and large heat capacity of lake water cause the later dates of FFF over the Great Lakes than over the southwestern part of the region. The second EOF mode for the FFS is found to be related to the spring PDO.

The explanations for the two leading modes of the three variables are only given statistically. Numerical experiments can be conducted to further validate the forcing of SST anomaly over North Pacific Ocean on the above-mentioned Rossby wave train. But the statistical relation is critical for developing seasonal predictions for the length of the FFS in the Great lakes region. Our research should be extended to the western United States where more noticeable lengthening of the FFS in recent years has been noted (Easterling, 2002).

Acknowledgements

This research is supported by the USDA Forest Service Northern Research Station and by AgBioResearch of Michigan State University.

References

Alonge CJ, Cosgrove BA. 2008. Application of NARR-based NLDAS ensemble simulations to continental-scale drought monitoring. AGU spring Meeting, H43E-6. Fort Lauderdate, FL.

Andresen JA, Winkler JA. 2009. *Weather and Climate*. Pearson Custom Publishing: Boston, MA.

Andresen J, Hilberg S, Kunkel K. 2012. Historical climate and climate trends in the midwestern USA. *Great Lakes Integrated Sciences and Assessments Center Occasional Paper #12002* (Prepared for the Midwest Technical Input Report, U.S. National Climate Assessment). http://glisa.msu.edu/docs/NCA/MTIT_Historical.pdf.

Barnston AG, Livezey RE. 1987. Classification, seasonality, and persistence of low-frequency atmospheric circulation patterns. *Mon. Weather Rev.* **115**(6): 1083–1126.

Cayan DR, Kammerdiener SA, Dettinger MD, Caprio JM, Peterson DH. 2001. Changes in the onset of spring in the western United States. *Bull. Am. Meteorol. Soc.* **82**: 399–415.

Changnon SA, Jones DMA. 1972. Review of the influences of the Great Lakes on weather. *Water Resour. Res.* **8**: 360–371.

Cook ER, D'Arrigo RD, Briffa KR. 1998. A reconstruction of the North Atlantic Oscillation using tree-ring chronologies from North America and Europe. *The Holocene* **8**: 9–17.

Cooter E, LeDuc S. 1995. Recent frost date trends in the northeastern United States. *Interannu. J. Climatol.* **15**: 65–75.

Cotton PA. 2003. Avian migration phenology and global climate change. *Proc. Natl. Acad. Sci.* **100**: 12219–12222.

DeGaetano AT. 1996. Recent trends in maximum and minimum temperature threshold exceedances in the northeastern United States. *J. Clim.* **9**(7): 1646–1657.

Ding Q, Wang B. 2005. Circumglobal teleconnection in the Northern Hemisphere summer. *J. Clim.* **18**(17): 3483–3505.

Easterling DR. 2002. Recent changes in frost days and the frost-free season in the United States. *Bull. Am. Meteorol. Soc.* **83**(9): 1327–1332.

Eichenlaub VL, Harman JR, Nurnberger FV, Stolle HJ. 1990. *The Climatic Atlas of Michigan*. University of Notre Dame Press: Notre Dame, IN.

Flore JA. 1994. Stone fruit. In Handbook of Environmental Physiology of Fruit Crops. Vol. I: Temperate Crops, Schaffer B, Andersen PC (eds). CRC Press: Boca Raton, FL; 96–97.

Groisman P, Knight RW, Karl TR, Easterling DR, Sun B, Lawrimore JH. 2004. Contemporary changes of the hydrological cycle over the contiguous United States: trends derived from in situ observations. *J. Hydrometeorol.* **5**(1): 64–85.

Higuchi K, Huang J, Shabbar A. 1999. A wavelet characterization of the north Atlantic Oscillation variation and its relationship to the northern Atlantic sea surface temperature. *Int. J. Climatol.* **19**(10): 1119–1129.

Huntington TG, Hodgkins GA, Keim BD, Dudley RW. 2004. Changes in the proportion of precipitation occurring as snow in New England (1949–2000). *J. Clim.* **17**(13): 2626–2636.

Kalnay E, Kanamitsu M, Kister R, Colins W, Deaven D, Gandin L, Iredell M, Saha S, White G, Woollen J, Zhu Y, Chelliah M, Ebisuzakl W, Higgins W, Janowiak J, Mo KC, Ropelewski C, Wang J, Leetmaa A, Reynolds R, Jenne R, Joseph D. 1996. The NCEP/NCAR 40-year reanalysis project. *Bull. Am. Meteorol. Soc.* **77**: 437–471.

Kanamitsu M, Ebisuzaki W, Woollen J, Yang S-K, Hnilo JJ, Fiorino M, Potter GL. 2002. NCEP/DOE AMIP-IIReanalysis (R-2). *Bull. Am. Meteorol. Soc.* **83**: 1631–1643.

Karl TR, Melillo JM, Peterson TC, Hassol SJ. 2009. Regional Climate Impacts: Midwest, Global Climate Change Impacts in the United States, U.S. Global Change Research Program. Cambridge University Press: Cambridge, UK.

Kister R, Collins W, Saha S, White G, Woollen J, Kalnay E, Chelliah M, Ebisuzaki W, Kanamitsu M, Kousky V, Dool H, Jenne R, Fiorino M. 2001. The NCEP-NCAR 50-year reanalysis: monthly means CD-ROM and documentation. *Bull. Am. Meteorol. Soc.* **82**: 247–267.

Kunkel KE, Easterling DR, Hubbard K, Redmond K. 2004. Temporal variations in frost-free season in the United States: 1895–2000. *Geophys. Res. Lett.* **31**: L03201, DOI: 10.1029/2003GL018624.

Luo L, Robock A, Mitchell KE, Houser PR, Wood EF, Schaake JC, Lohmann D, Cosgrove B, Wen F, Sheffield J, Duan Q, Higgins RW, Pinker RT, Tarpley JD. 2003. Validation of the North American Land Data Assimilation System (NLDAS) retrospective forcing over the Southern Great Plains. *J. Geophys. Res.* **108**: 8843, DOI: 10.1029/2002JD003246.

Mann HB. 1945. Non-parametric test against trend. *Econometrika* **13**: 245–259.

Mantua NJ, Hare SR, Zhang Y, Wallace JM, Francis RC. 1997. A Pacific interdecadal climate oscillation with impacts on salmon production. *Bull. Am. Meteorol. Soc.* **78**: 1069–1079.

Mesinger F, DiMego G, Kalnay E, Mitchell K, Shafran PC, Ebisuzaki W, Jovic D, Woollen J, Rogers E, Berbery EH, Ek MB, Fan Y, Grumbine R, Higgins W, Li H, Lin Y, Manikin G, Parrish D, Shi W. 2006. North American regional reanalysis. *Bull. Am. Meteorol. Soc.* **87**: 343–360.

Mitchell KE, Lohmann D, Houser PR, Wood EF, Schaake JC, Robock A, Cosgrove BA, Sheffield J, Duan Q, Luo L, Higgins RW, Pinker RT, Tarpley JD, Lettenmaier DP, Marshall CH, Entin JK, Pan M, Shi W, Koren V, Meng J, Ramsay BH, Bailey AA. 2004. The multi-institution North American Land Data Assimilation System (NLDAS): utilizing multiple GCIP products and partners in a continental distributed hydrological modeling system. *J. Geophys. Res.* **109**: D07S90, DOI: 10.1029/2003JD003832.

MRCC. 2013. *Regional Median Freeze Maps*, *Regional Climatology Series*. Midwestern Regional Climate Center, Champaign, IL. Accessed on 30 April 2013. http://mcc.sws.uiuc.edu/cliwatch/frz_maps_spring/DLY_FRZ_REGL_MAPS.htm

Nemani RR, White MA, Cayan DR, Jones GV, Running SW, Coughlan JC, Peterson DL. 2001. Asymmetric warming over coastal California and its impact on the premium wine industry. *Clim. Res.* **19**: 25–34.

Nicholls N. 2005. Climate variability, climate change and the Australian snow season. *Aust. Meteorol. Magazine* **54**: 177–185.

Pan M, Sheffield J, Wood EF, Mitchell KE, Houser PR, Schaake JC, Robock A, Lohmann D, Cosgrove B, Duan Q, Luo L, Higgins RW, Pinker RT, Tarpley JD. 2003. Snow process modeling in the North American Land Data Assimilation System (NLDAS): 2. Evaluation of model simulated snow water equivalent. *J. Geophys. Res* **108**(D22): 8850, DOI: 10.1029/2003JD003994.

Peng S, Whitaker JS. 1999. Mechanism determining the atmospheric response to mid latitude SST anomalies. *J. Clim.* **12**(5): 1393–1408.

Peng S, Robinson WA, Hoerling MP. 1997. The modeled atmospheric response to midlatitude SST anomalies and its dependence on background circulation states. *J. Clim.* **10**(5): 971–987.

Schneider U, Schonwiese CD. 1989. Some statistical characteristics of the El Nino/Southern Oscillation and North Atlantic Oscillation indices. *Atmosfera* **2**: 167–180.

Schwartz MD, Reiter BE. 2000. Changes in North American spring. *Int. J. Climatol.* **20**: 929–932.

Scott RW, Huff FA. 1997. Lake effects on climatic conditions in the Great Lakes basin. MCC Research Report 97–10, Illinois State Water Survey Atmospheric Sciences Division. Champaign, IL, 35–47.

Sheffield J, Pan M, Wood EF, Mitchell KE, Houser PR, Schaake JC, Robock A, Lohmann D, Cosgrove B, Duan Q, Luo L, Higgins RW, Pinker RT, Tarpley JD, Ramsay BH. 2003. Snow process modeling in the North American Land Data Assimilation System (NLDAS): 1. Evaluation of model-simulated snow cover extent. *Journal of Geophysical Research* **108**(D22): 8849, DOI: 10.1029/2002JD003274.

Stephanie AM, Russell JI. 2008. Northern Annular Mode impact on spring climate in the western United States. *Geophys. Res. Lett.* **35**: L17701, DOI: 10.1029/2008GL034828.

Stewart IT, Cayan DR, Dettinger MD. 2004. Changes toward earlier stream flow timing across western North America. *J. Clim.* **18**(8): 1136–1155.

USDA NASS. 2013. Crop Values *2012* Summary. U.S. Department of Agriculture National Agricultural Statistics Service: Washington, DC.

Wallace JM, Gutzler D. 1981. Teleconnection in the geopotential height field during the Northern Hemisphere winter. *Mon. Weather Rev.* **109**: 784–812.

Wang J, Bai X, Hu H, Clites A, Colton M, Lofgren B. 2012. Temporal and spatial variability of Great Lakes ice cover, 1973–2010. *J. Clim.* **25**(4): 1318–1329.

Winkler J, Andresen J, Bisanz J, Black R, Guentchev G, Nugent J, Piromsopa K, Rothwell N, Zavalloni C, Clark J, Min H, Pollyea A, Prawiranata H, Torre R. 2013. Michigan's Tart Cherry Industry: vulnerability to climate variability and change (Chapter 8). In Climate Change Impacts, Risk, Vulnerability, and Adaptation in the Midwestern United States, Pryor SC (ed). Indiana University Press: Bloomington, IN; 104–116.

Zhang Y, Wallace JM, Basttisti DS. 1997. ENSO-like interdecadal variability: 1900–93. *J. Clim.* **10**: 1004–1020.

Zhou LM, Tucker CJ, Kaufmann PK, Slayback D, Shabanov NV, Myneni RB. 2001. Variations in northern vegetation activity inferred from satellite data of vegetation index during 1981 to 1999. *J. Geophys. Res.* **106**: 20069–20084.

